

Single-stranded Adenine-rich DNA and RNA Retain Structural Characteristics of their Respective Double-stranded Conformations and Show Directional Differences in Stacking Pattern

*J. Isaksson, S. Acharya, J. Barman, P. Cheruku and J. Chattopadhyaya**

Department of Bioorganic Chemistry, Box 581, Biomedical Center, Uppsala University, S-751 23

Uppsala, Sweden

E-mail: jyoti@boc.uu.se

Table of contents

1. **Table S1.** A summary of all inter-proton distances used for structure evaluation of DNA and RNA. The distances have been measured in one strand of canonical model builds of A-, B- and Z-type conformations. The right columns show the observed cross-peak intensities for ssDNA (**1a**) and ssRNA (**1b**) respectively, categorized as strong, medium, or weak intensities.
2. **Table S2.** (A) The dihedral- and sugar phaseangle constraints used in the molecular modelling simulation of ssDNA (**1a**). (B) The dihedral- and sugar phase angle constraints used in the molecular modeling simulation of ssRNA (**1b**).

3. **Table S3.** Comparison of Nucleobase-dependent pK_a and $\Delta G_{pK_a}^o$ ^b of the 9-guanylate ions in ssDNAs (left) and ssRNAs (right).
4. **Table S4.** 1H chemical shifts [δ_H , ppm] at neutral (N) and the deprotonated (D) states at 298 K for monomeric- (2a, 2b, 3a, 3b, 4a, 4b) and hexameric (1a, 1b) ssDNA and ssRNA.
5. **Figure S1:** Panels (A–G) show NMR assignments for compounds **1a** and **1b**. Proton and phosphate assignments are shown in each spectrum.
6. **Figure S2.** Oligomerization shifts at 298 K for aromatic marker protons of the individual nucleotide residues in ssDNAs (**1a**) and ssRNAs (**1b**) with respect to their corresponding monomeric 2'-deoxy 3'-ethylphophates (dNpEt or EtpdNpEt or EtpdN) and ribo- 3'-ethylphophates (rNpEt or EtprNpEt or EtprN) respectively.
7. **Figure S3:** The inter-residue crosspeaks used in the structure generation for ssDNA (**1a**) compared to ssRNA (**1b**). Strong peaks were assigned to 3.4 (± 1.6) Å and weak peaks were allowed a considerable contribution from spin-diffusion and were assigned to 4.4 (-1.4/+1.6) Å.
8. **Figure S4.** (A) A comparison of the backbone dihedrals of the average structures of the final 100 ps of the MD simulation between ssDNA (**1a**) and the ssRNA (**1b**). The average structure of the MD trajectory of the last 100 ps was based on one coordinate set per 0.15 ps, and minimized for 2000 steps using the conjugate gradient method and full NMR constraints switched on. As expected, the major differences are found for base χ torsion and the sugar phase angle (P), where ssDNA takes up the characteristic B-form, and the ssRNA takes up the characteristic A-form. For reference, the average values^{1a} of canonical double-stranded A-type RNA (dotted) and canonical double-stranded B-type DNA (dashed) have been plotted in the graphs. (B) A comparison between the single-strand helical parameters of the average (see experimental section) ssDNA (**1a**) and the ssRNA (**1b**) structures.
9. **Figure S5.** The temperature-dependent drift of the ssDNA and ssRNA aromatic protons due to kinetically driven destacking.
10. **Figure S6.** The shielding coefficient of the imino proton of **G** calculated using the stacking pattern for d**G**AAAAAC and r**G**AAAAAC plotted versus the pK_a .

Table S1. Summary of all inter-proton distances of interest for evaluation of DNA and RNA structures. The distances have been measured in one strand of canonical model builds of A-, B- and Z-type conformations. The right columns show the observed crosspeak intensities for ssDNA and ssRNA respectively, categorized as strong, medium or weak intensities. Shaded lines are used to highlight found differences between the ssDNA and the ssRNA sample.

	Inter-residue distances in canonical RNA/DNA			NOE crosspeaks	
inter-resid distance	dsB-d/rNA	dsA-d/rNA	dsZ-d/rNA	ssDNA	ssRNA
H6/H8 _(n) -H6/H8 _(n-1)	5.05	4.60	6.03	w	w
H6/H8 _(n) -H1' _(n-1)	3.01	4.34	6.98	s	s
H6/H8 _(n) -H2' _(n-1)	3.52	2.05	7.89	s	s
H6/H8 _(n) -H2'' _(n-1)	2.29	2.96	8.04	s	#
H6/H8 _(n) -H3' _(n-1)	5.10	3.25	6.89	m	s
H6/H8 _(n) -H4' _(n-1)	6.03	5.21	4.76	m	m
H6/H8 _(n) -H5'' _(n-1)	7.25/6.89	6.15/6.73	3.31/4.66	-/-	-/-
H2 _(n) -H1' _(n+1)	4.64	3.48	5.20	m	s
H5 _(n) -H6/H8 _(n-1)	3.64	3.44	5.15	m	m
H5 _(n) -H2'' _(n-1)	3.15/3.10	3.17/4.78	3.01/4.42	m/m	m/#
H5 _(n) -H1' _(n-1)	3.80	5.00	5.18	m	w
H5 _(n) -H3' _(n-1)	5.47	3.70	4.41	w	m
H2 _(n) -H5'' _(n+1)	4.87/6.48	6.64/7.80	6.66/6.74	-/-	-/-
H2 _(n) -H4' _(n+1)	5.69	6.32	6.81	w	-
H2 _(n) - H2'' _(n+1)	6.83/6.22	5.32/6.19	10.37/11.74	-/-	w/#

	Intra-residue distances in canonical RNA/DNA			NOE crosspeaks	
IntraResid Distance	dsB-d/rNA	dsA-d/rNA	dsZ-d/rNA	ssDNA	ssRNA
H6/H8 _(n) -H2 _(n)	4.28	4.49	4.23	w	w
H6/H8 _(n) -H1' _(n)	3.84	3.73	3.48	s	s
H6/H8 _(n) -H2' _(n)	2.74	3.43	3.92	s	s
H6/H8 _(n) -H2'' _(n)	3.69	4.91	4.38	s	#
H6/H8 _(n) -H3' _(n)	4.37	3.24	5.13	m	s

H6/H8 _(n) -H4' _(n)	4.92	4.61	5.03	m	m
H6/H8 _(n) -H5' _(n)	4.54/3.57	4.62/4.11	5.21/4.19	m	w
H2 _(n) -H1' _(n)	4.28	4.49	4.23	w	w
H2 _(n) -H2' _(n)	7.02/5.84	4.63/5.38	5.83/4.63	-/w	m/#
H2 _(n) -H3' _(n)	8.26	6.96	7.48	-	-
H2 _(n) -H4' _(n)	7.26	7.61	7.60	w	-
H2 _(n) -H5' _(n)	8.38/8.72	8.98/9.29	9.18/8.84	-	-
H5 _(n) -H1' _(n)	5.40	5.30	5.29	w	w
H5 _(n) -H2' _(n)	4.64/5.47	4.84/6.52	5.44/5.87	m/w	m/#
H5 _(n) -H3' _(n)	6.38	4.87	7.00	w	m
H5 _(n) -H4' _(n)	6.78	6.56	6.93	w	-

-- not detectable

w - weak (4 - 5 Å)

m - medium (2.5 - 4 Å)

s - strong (<3 Å)

- RNA is devoid of H2"

NOESY: $\tau_m = 800\text{ms}$, T = 278 K (DNA), 283 K (RNA), 4k x 1k x 32 complex datapoints.

Table S2A. The dihedral- and sugar phase angle constraints used in the molecular modeling simulation of ssDNA (**1a**).

	dG	dA ¹	dA ²	dA ³	dA ⁴	dC
α	-	-	-	-	-	-
β	-	140-220°	140-220°	140-220°	140-220°	140-220°
γ	20-100°	20-100°	20-100°	20-100°	20-100°	20-100°
ε	140-220°	140-220°	140-220°	140-220°	140-220°	-
ζ	-	-	-	-	-	-
P	120-210°	120-210°	120-210°	120-210°	120-210°	0-210°

Table S2B. The dihedral- and sugar phase angle constraints used in the molecular modeling simulation of ssRNA (**1b**).

	rG	rA ¹	rA ²	rA ³	rA ⁴	rC
α	-	-	-	-	-	-
β	-	140-220°	140-220°	140-220°	140-220°	140-220°
γ	20-100°	20-100°	20-100°	20-100°	20-100°	20-100°
ε	140-340°	140-340°	140-340°	140-340°	140-340°	-
ζ	-	-	-	-	-	-
P	0-210°	0-210°	0-120°	0-120°	0-120°	0-120°

Table S3. Comparison of Nucleobase-dependent pK_a ^a and $\Delta G_{pK_a}^o$ ^b of the 9-guanylate ion in ssDNAs (left) and ssRNAs (right).

Oligo-ssDNA	pK_a	$\Delta G_{pK_a}^o$	Oligo-ssRNA	pK_a	$\Delta G_{pK_a}^o$
dGpEt	9.40 (± 0.02), H8G	53.6 (± 0.1)	rGpEt	9.25 (± 0.02), H8G	52.8 (± 0.1)
d(GA)	G 9.45 (± 0.01), H8G A 9.44 (± 0.01), H2A	53.9 (± 0.1) 53.9 (± 0.1)	r(GA)	G 9.17 (± 0.02), H8G A 9.11 (± 0.02), H8A	52.4 (± 0.1) 52.0 (± 0.1)
d(GC)	G 9.35 (± 0.01), H8G C 9.33 (± 0.01), H5C	53.3 (± 0.1) 53.2 (± 0.1)	r(GC)	G 9.56 (± 0.01), H8G C 9.56 (± 0.01), H5C	54.5 (± 0.1) 54.5 (± 0.1)
d(GAC)	G 9.64 (± 0.02), H8G A 9.53 (± 0.02), H2A C 9.63 (± 0.03), H5C	55.0 (± 0.1) 54.4 (± 0.1) 54.9 (± 0.2)	r(GAC)	G 9.88 (± 0.02), H8G A 9.88 (± 0.02), H2A C 9.89 (± 0.02), H5C	56.4 (± 0.1) 56.4 (± 0.1) 56.4 (± 0.1)
d(GA ¹ A ² C)	G 9.87 (± 0.01), H8G A ¹ 9.92 (± 0.03), H8A A ² 9.77 (± 0.03), H2A C 9.82 (± 0.01), H5C	56.3 (± 0.1) 56.6 (± 0.1) 55.7 (± 0.2) 56.0 (± 0.1)	r(GA ¹ A ² C)	G 9.76 (± 0.01), H8G A ¹ 9.73 (± 0.02), H8A A ² 9.71 (± 0.02), H8A C 9.70 (± 0.02), H5C	55.7 (± 0.1) 55.5 (± 0.1) 55.4 (± 0.1) 55.3 (± 0.1)
d(GA ¹ A ² A ³ C)	G 10.11 (± 0.01), H8G A ¹ 10.18 (± 0.02), H8A A ² - A ³ - C -	57.7 (± 0.1) 58.1 (± 0.2) - - -	r(GA ¹ A ² A ³ C)	G 9.82 (± 0.01), H8G A ¹ 9.73 (± 0.01), H8A A ² 9.76 (± 0.01), H8A A ³ 9.68 (± 0.03), H8A C 9.63 (± 0.03), H6C	56.0 (± 0.1) 55.5 (± 0.1) 55.7 (± 0.1) 55.2 (± 0.2) 54.9 (± 0.2)
d(GA ¹ A ² A ³ A ⁴ C)	G 9.93 (± 0.01), H8G A ¹ - A ² - A ³ 9.80 (± 0.02), H2A A ⁴ - C -	56.7 (± 0.1) 57.1 (± 0.2) 56.0 (± 0.1) 55.9 (± 0.1) - -	r(GA ¹ A ² A ³ A ⁴ C)	G 9.76 (± 0.01), H8G A ¹ 9.65 (± 0.01), H8A A ² 9.95 (± 0.01), H8A A ³ 10.50 (± 0.07), H2A A ⁴ - C 10.18 (± 0.03), H6C	55.7 (± 0.1) 55.1 (± 0.1) 56.8 (± 0.1) 59.9 (± 0.4) - 58.1 (± 0.2)

^a All pK_a values and the corresponding errors have been calculated by Hill plot analysis

^b $\Delta G_{pK_a}^o$ have been calculated using the relation: $\Delta G_{pK_a}^o = 2.303 * RT * pK_a$

Table S4. ^1H chemical shifts [δ_{H} , ppm] at neutral (N) and the deprotonated (D) states at 298 K for monomeric- (2a, 2b, 3a, 3b, 4a, 4b) and hexameric (1a, 1b) ssDNA and ssRNA.

Compounds	^1H Chemical Shift [δ_{H}] at neutral (N) and deprotonated (D) ^c states at 298 K							
	$\delta_{\text{H}8}$		$\delta_{\text{H}2}$		$\delta_{\text{H}6}$		$\delta_{\text{H}5}$	
	N	D	N	D	N	D	N	D
dGpEt (2a)	7.998	<i>7.865</i>	-	-	-	-	-	-
EtpdApEt (3a)	8.464	<i>8.464</i>	8.277	<i>8.277</i>	-	-	-	-
5'-EtpdC (4a)	-	-	-	-	7.925	7.925	6.092	6.092
rGpEt (2b) ^{b,c}	.010	<i>7.861</i>	-	-	-	-	-	-
EtprApEt (3b) ^c	.493	<i>8.493</i>	3.284	<i>8.283</i>	-	-	-	-
5'-EtprC (4b) ^c	-	-	-	-	7.934	7.933	5.100	<i>6.099</i>
(1a)	G	7.701	<i>7.490</i>	-	-	-	-	-
	A¹	8.090	<i>8.082</i>	7.716	<i>7.700</i>	-	-	-
	A²	8.041	<i>8.049</i>	7.506	<i>7.522</i>	-	-	-
	A³	8.018	<i>8.019</i>	7.542	<i>7.553</i>	-	-	-
	A⁴	8.159	<i>8.158</i>	7.752	<i>7.759</i>	-	-	-
	C	-	-	-	-	7.638	7.639/7.543	5.751
(1b) ^c	G	.875	<i>7.720</i>	-	-	-	-	-
	A¹	.206	<i>8.242</i>	7.905	<i>7.880</i>	-	-	-
	A²	.091	<i>8.142</i>	7.827	<i>7.808</i>	-	-	-
	A³	.000	<i>7.999</i>	7.817	<i>7.805</i>	-	-	-
	A⁴	.969	<i>7.963</i>	3.058	<i>8.052</i>	-	-	-
	C	-	-	-	-	7.558	7.543	5.508

^a The chemical shifts at the deprotonated (D) state are given in *italic*. Internal standard: DSS ($\delta_{\text{DSS}} = 0.015$ ppm).

^b Data are taken from ref. 6d and 6e.

^c Data are taken from ref. 8f.

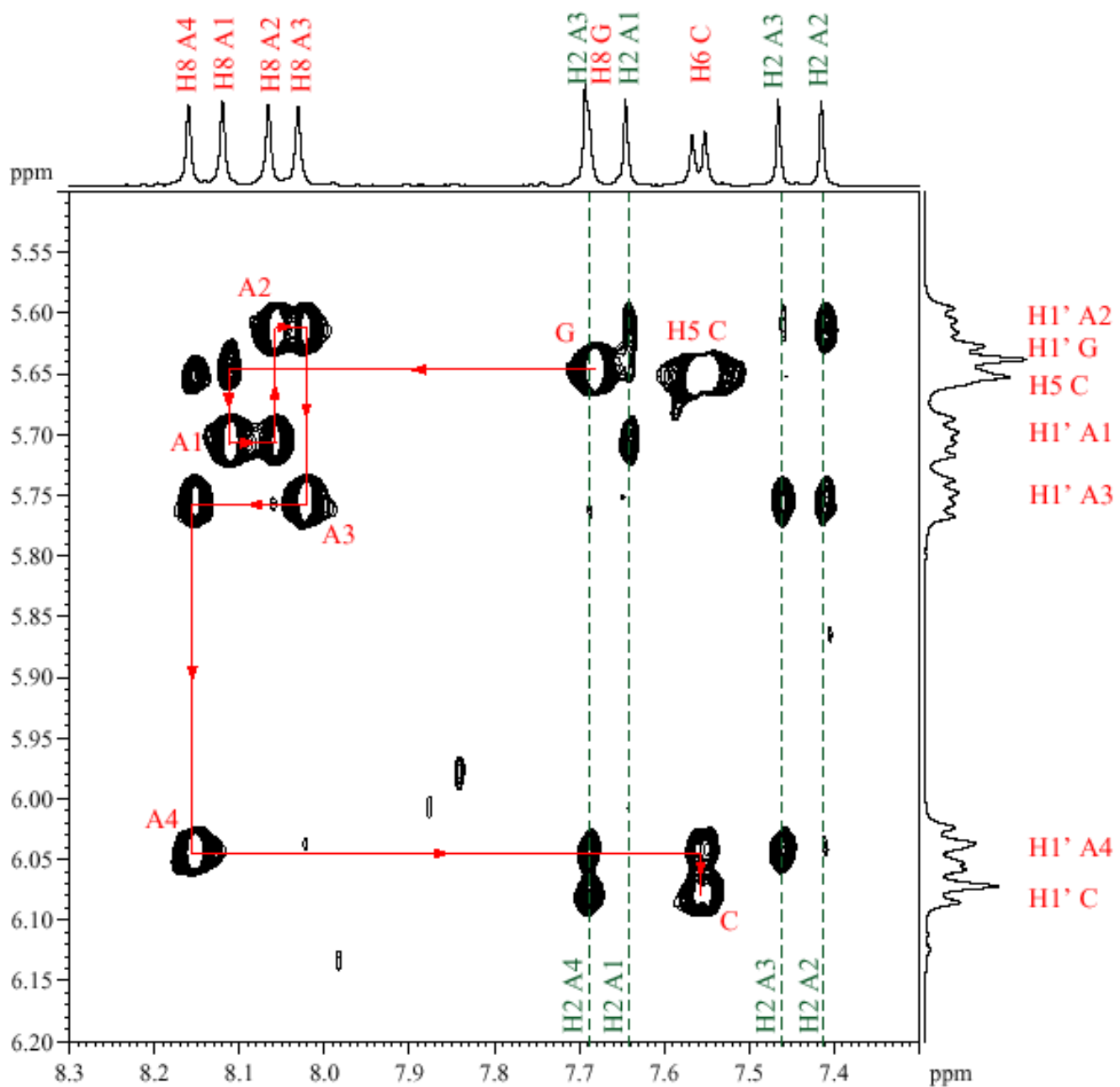


Figure S1: Panel A. The aromatic (7.3 - 8.3 ppm in F2) to $\text{H}^{1\prime}$ (5.4 – 6.2 ppm in F1) region of the $d(\text{GA}^1\text{A}^2\text{A}^3\text{A}^4\text{C})$ (**1a**) in a 800 ms NOESY spectrum at 278 K, clearly showing the sequential $\text{H}8/\text{H}6_n$ to $\text{H}^{1\prime}_{n-1}$ connectivity (red) and the H2 proton assignment (green). For the corresponding spectrum of the ssRNA, see ref 8f.

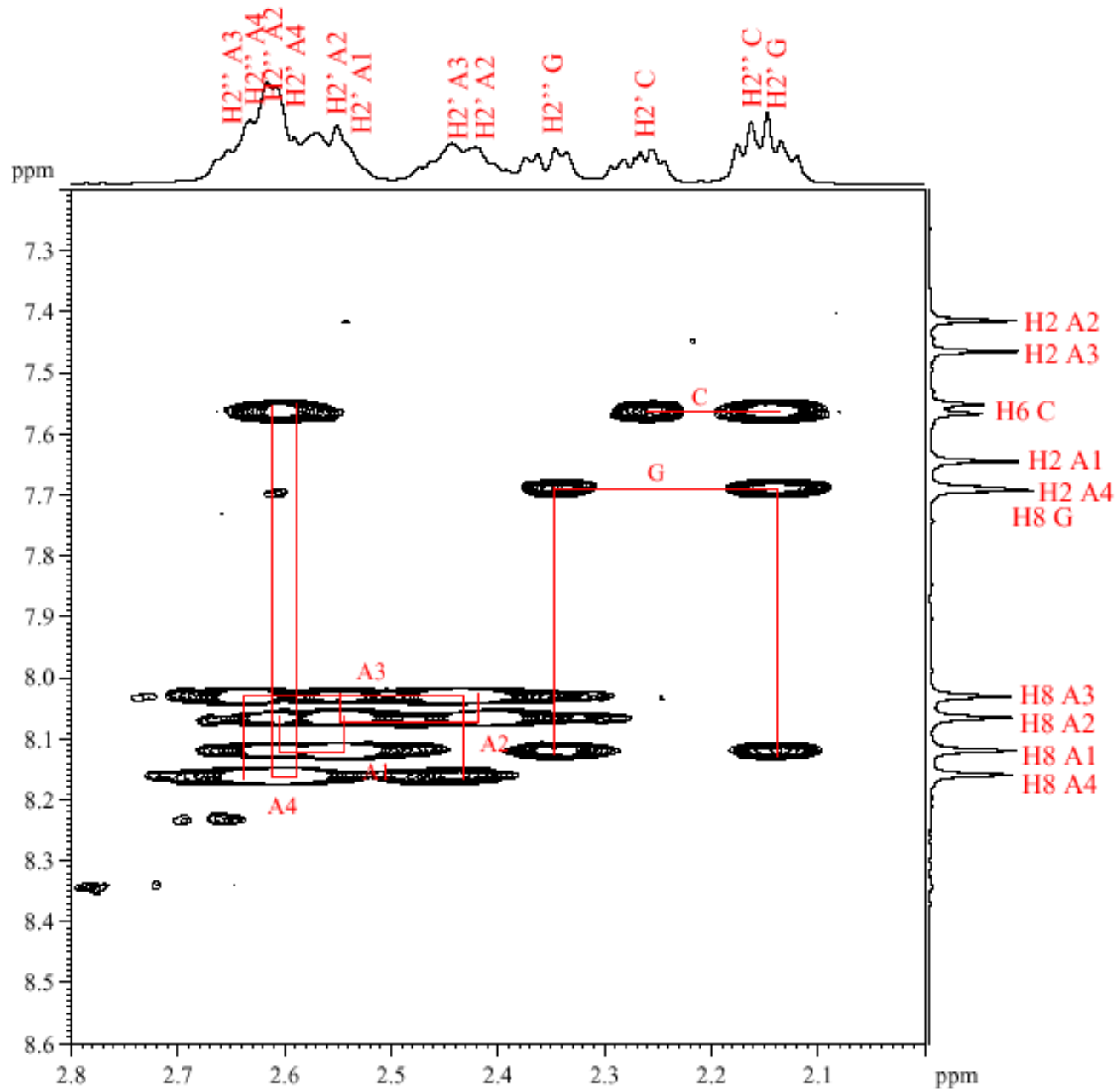


Figure S1: Panel B. The aromatic (7.2 – 8.6 ppm in F1) to H2'/H2" (2.0 – 2.8 ppm in F2) region of the d(GA¹A²A³A⁴C) (**1a**) in a 800 ms NOESY spectrum at 278 K, clearly showing the sequential H8/H6_n to H2''_{n-1} connectivity (red). For the corresponding spectrum of the ssRNA, see ref 8f.

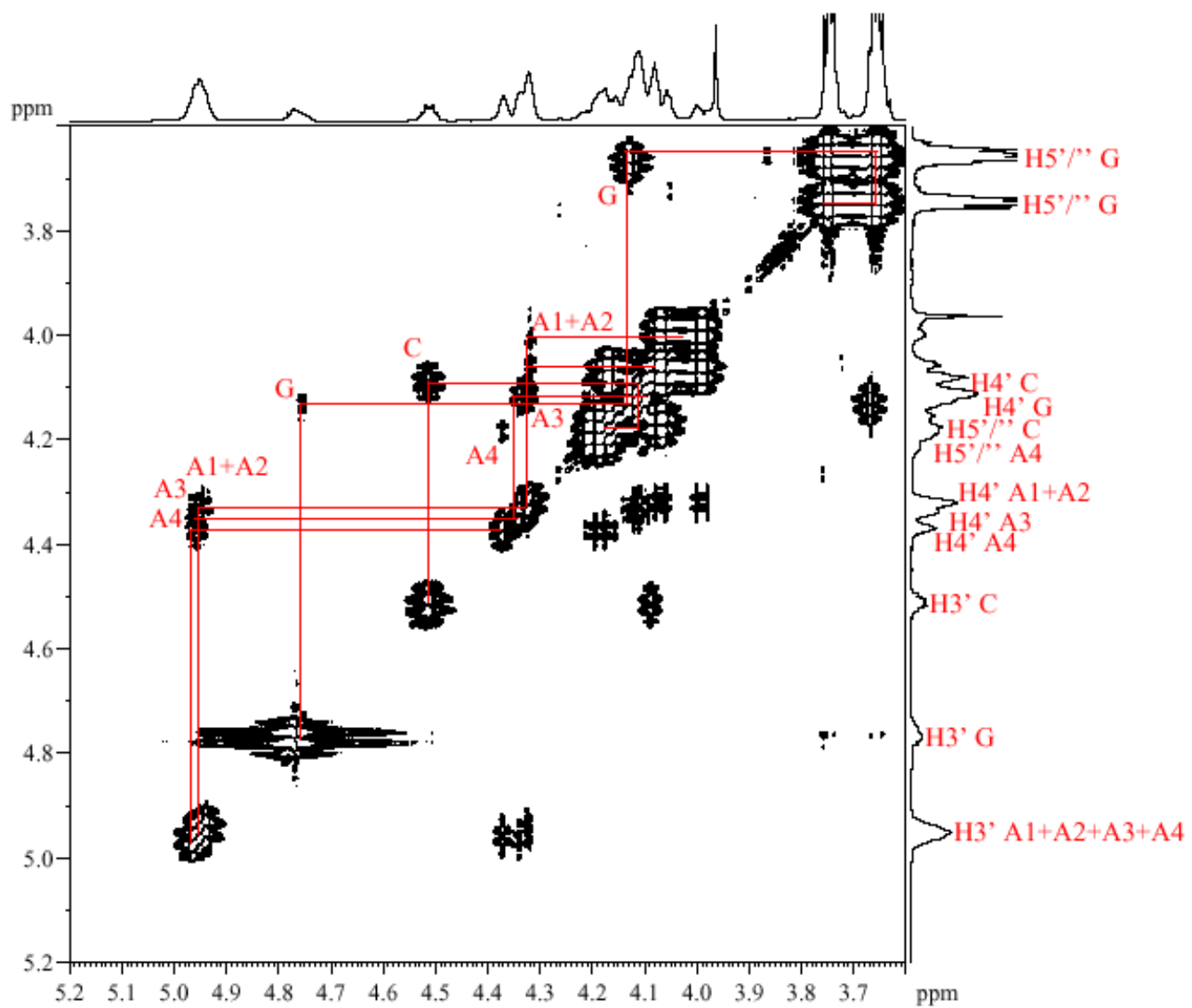


Figure S1: Panel C3. DQF-COSY {³¹P} of the H3', H4', H5'' region (3.6 – 5.2 ppm in F1 and F2) of the d(GA¹A²A³A⁴C) (**1a**). The cross-peaks show the assignment of the J-coupled sugar protons at 298 K (red).

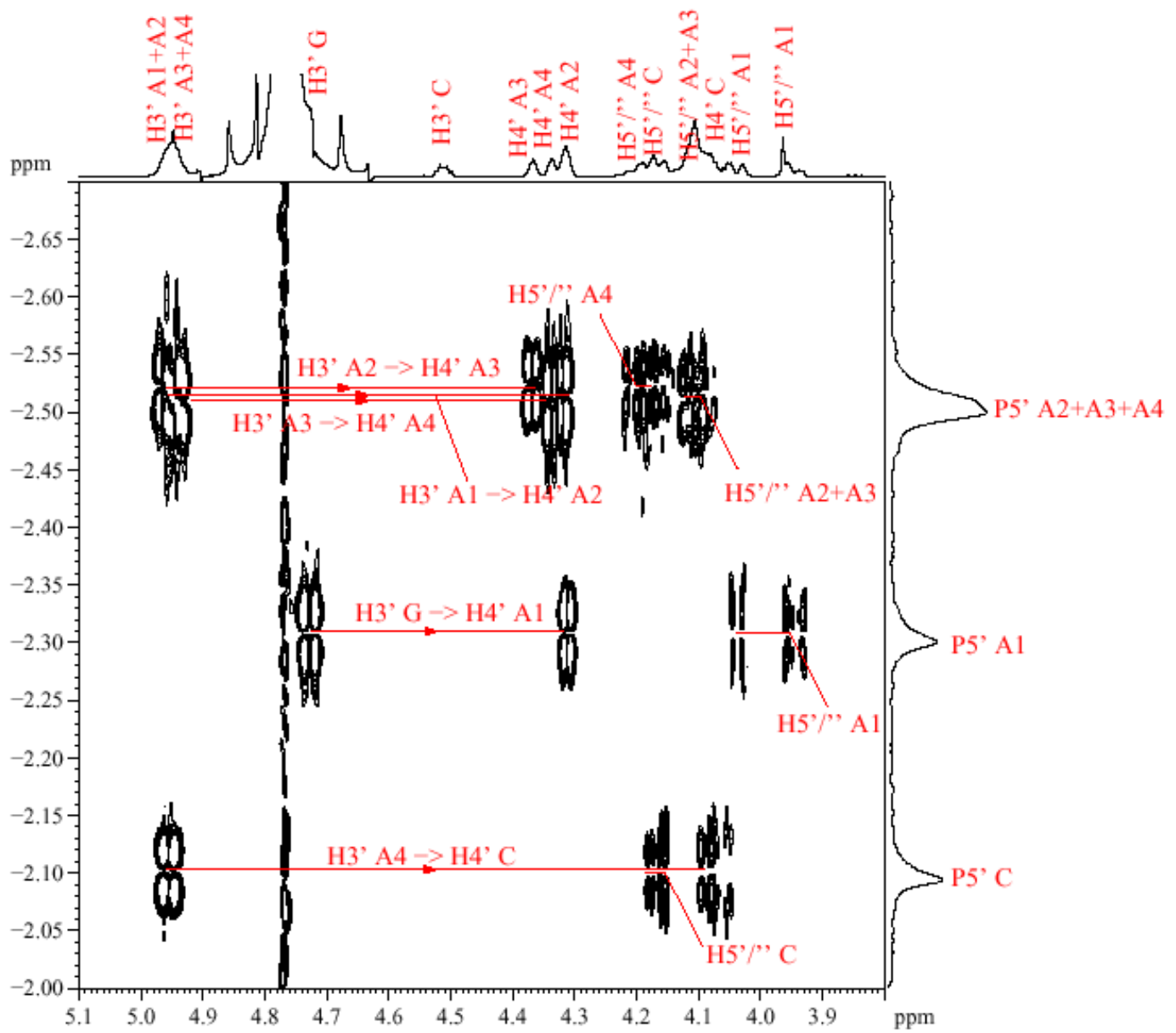


Figure S1: Panel D. The ^{31}P - ^1H correlation spectrum of d(GA $^1\text{A}^2\text{A}^3\text{A}^4\text{C}$) (**1a**) shows the assignment of the phosphates at 298 K (red). The presence of $^4J_{\text{H}_4'\text{P}}$ for all residues proves that the backbone spends a significant amount of time in a W-shape conformation where the affected backbone dihedral angles are in β^t and γ^+ . The absence of any $^4J_{\text{H}_2'\text{P}}$ correlations prove in a similar way that there are no significant ε^- conformations (see ref. 1a). Since ε^+ is sterically forbidden, ε^t is dominant. For the corresponding spectrum of the ssRNA, see ref 8f.

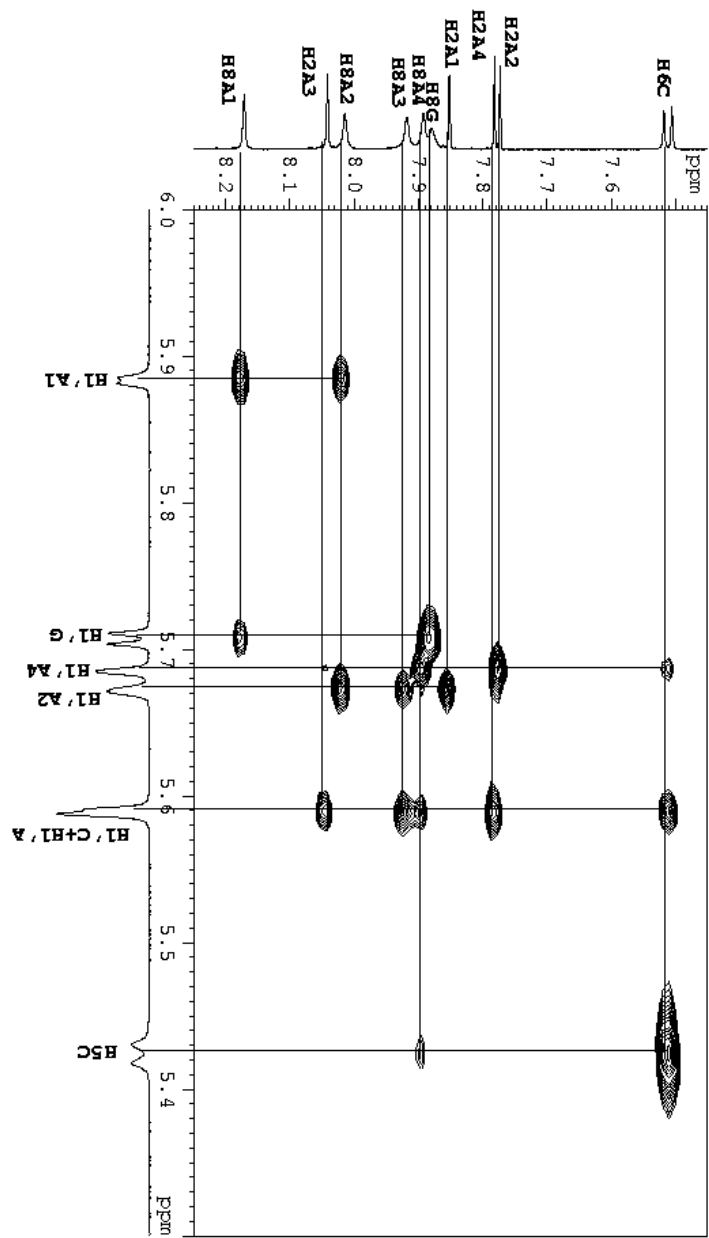


Figure S1 Panel E. Expanded NOESY spectra (mixing time $\tau = 800$ ms) of the aromatic (H₆/H₈/H₂) region (8.15 – 7.45 ppm in F1 direction) to the anomeric (H_{1'}) region (6.0 – 5.3 ppm in F2 direction) for r(GA¹A²A³A⁴C) (**1b**) at 283 K.

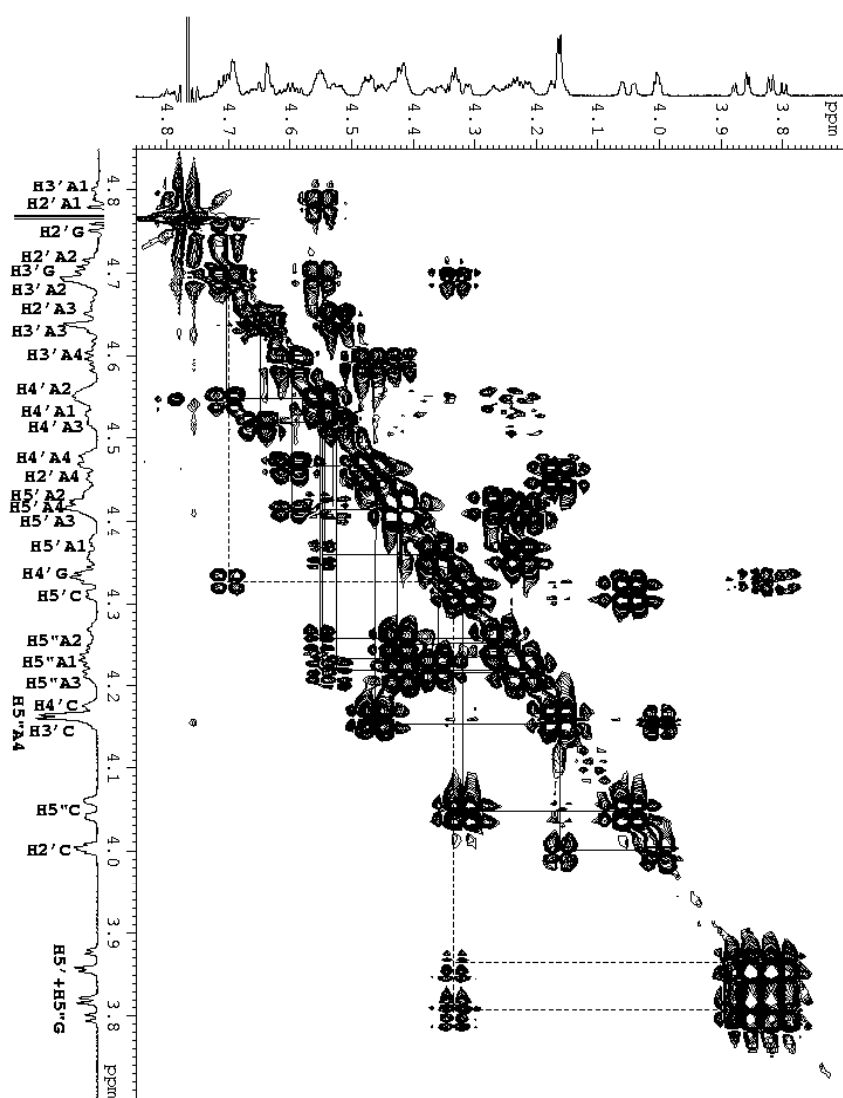


Figure S1 Panel F. Expanded DQF-COSY spectra of H2'/H3'/H4'/H5'/H5'' region (4.85 – 3.7 ppm in F1 direction) to H2'/H3'/H4'/H5'/H5'' region (4.85 – 3.7 ppm in F2 direction) for r(GA¹A²A³A⁴C) (**1b**) at 298 K.

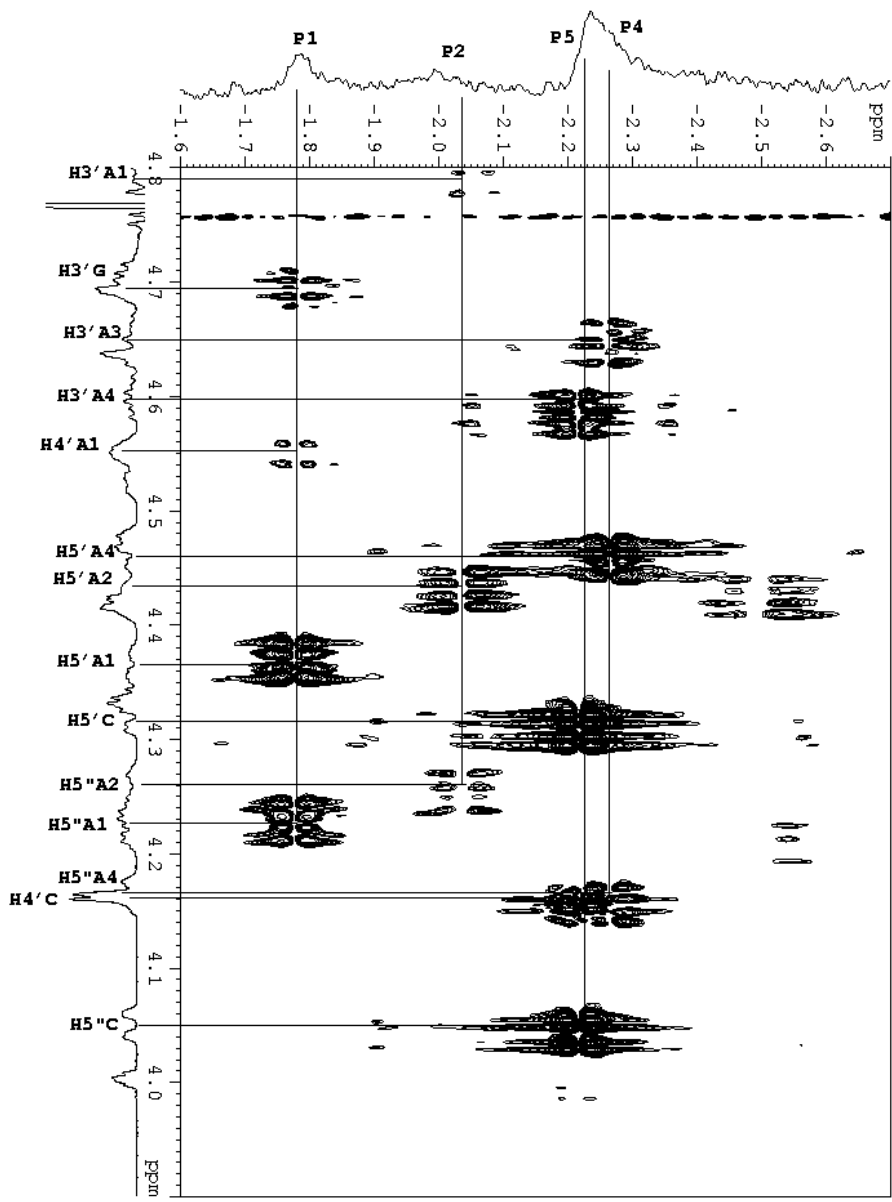


Figure S1 Panel G. Expanded ^{31}P - ^1H correlation spectroscopy of ^{31}P region (-1.6 – 2.5 ppm in F1 direction) to H2'/H3'/H4'/H5'/H5" region (4.8 – 3.9 ppm in F2 direction) for r(GA¹A²A³A⁴C) (**1b**) at 298 K

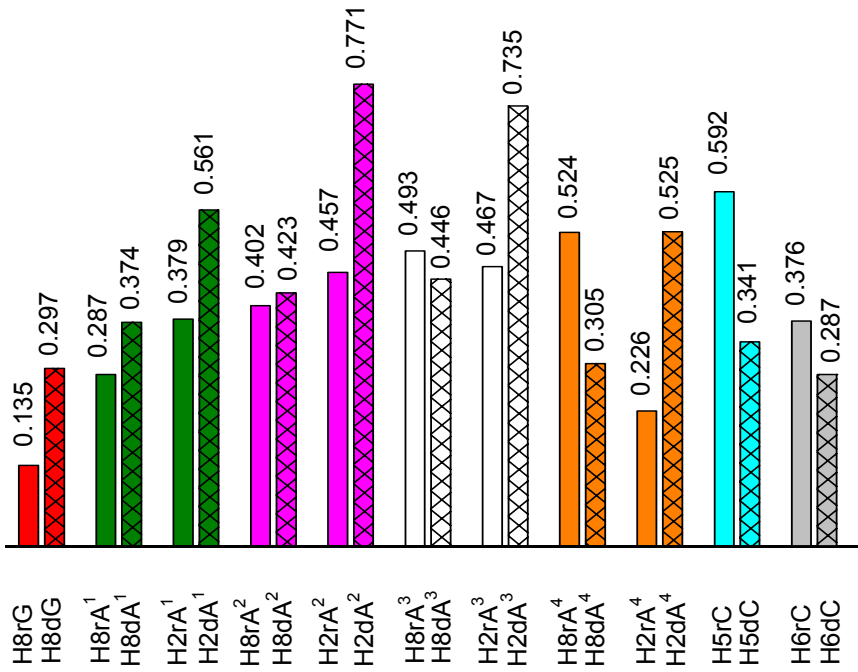


Figure S2. Oligomerization shifts^{5b,c} are calculated for the individual nucleotide residues in the oligos (O_{oligo}) with respect to the monomeric 2'-deoxy 3'-ethylphophates (NpEt or EtpNpEt or EtpN) [*i.e.* the difference of chemical shift: $\Delta\delta_{(\text{NpEt/EtpNpEt/EtpN} - O_{\text{oligo}})}$, in ppm, at 298 K]. The protons for ssRNA are shown in hollow columns (□), while those of the ssDNA are shown in crossed columns (☒). The different magnitudes of upfield shifts (*i.e.* differential anisotropic shielding) of the different protons show how that particular proton feels the aromatic ring current of the nearest neighbour.

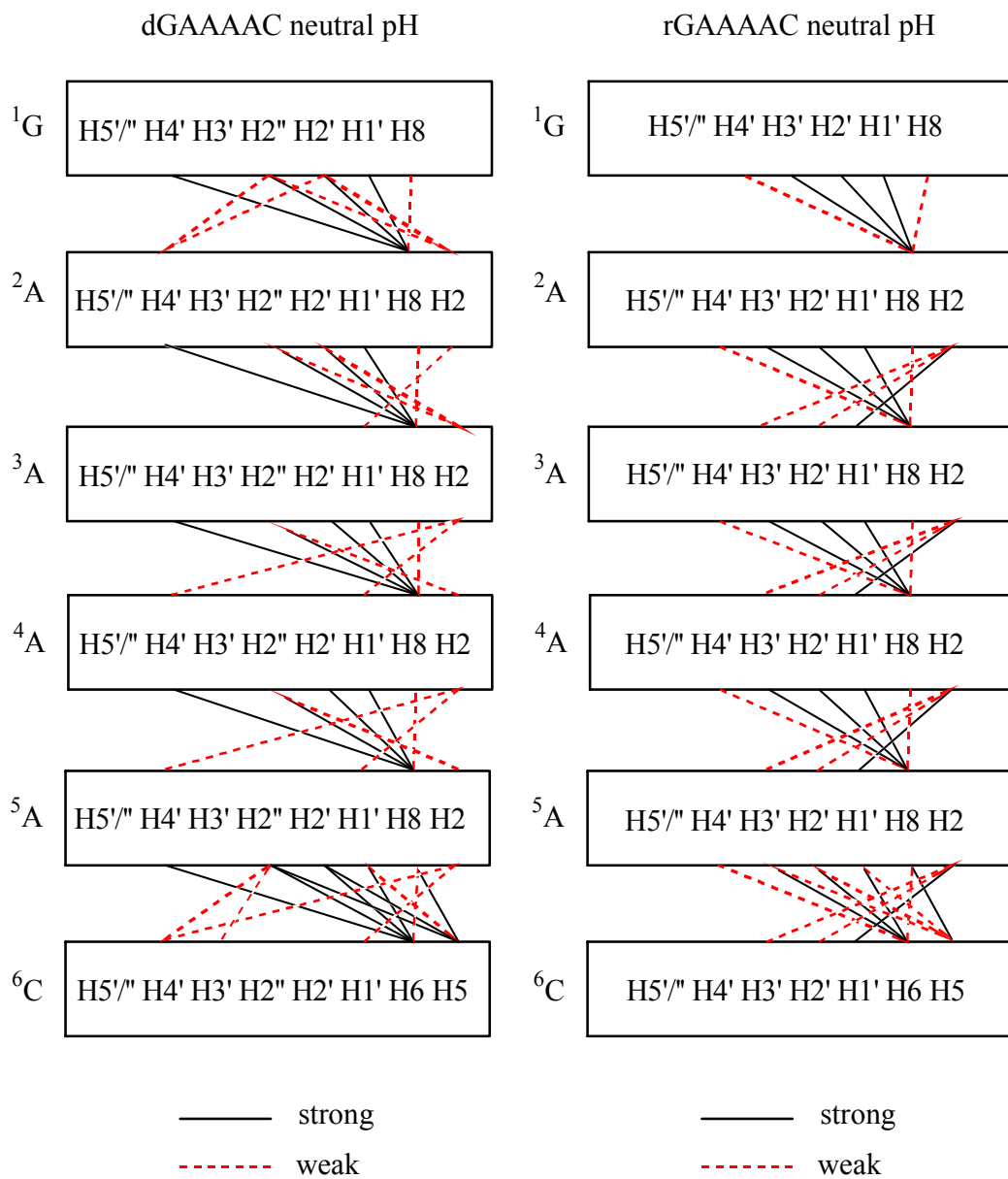


Figure S3. The inter-residue crosspeaks used in the structure generation for ssDNA (**1a**) compared to ssRNA (**1b**). Strong peaks were assigned to 3.4 (± 1.6) Å and weak peaks were allowed a considerable contribution from spin-diffusion and were assigned to 4.4 (-1.4/+1.6) Å.

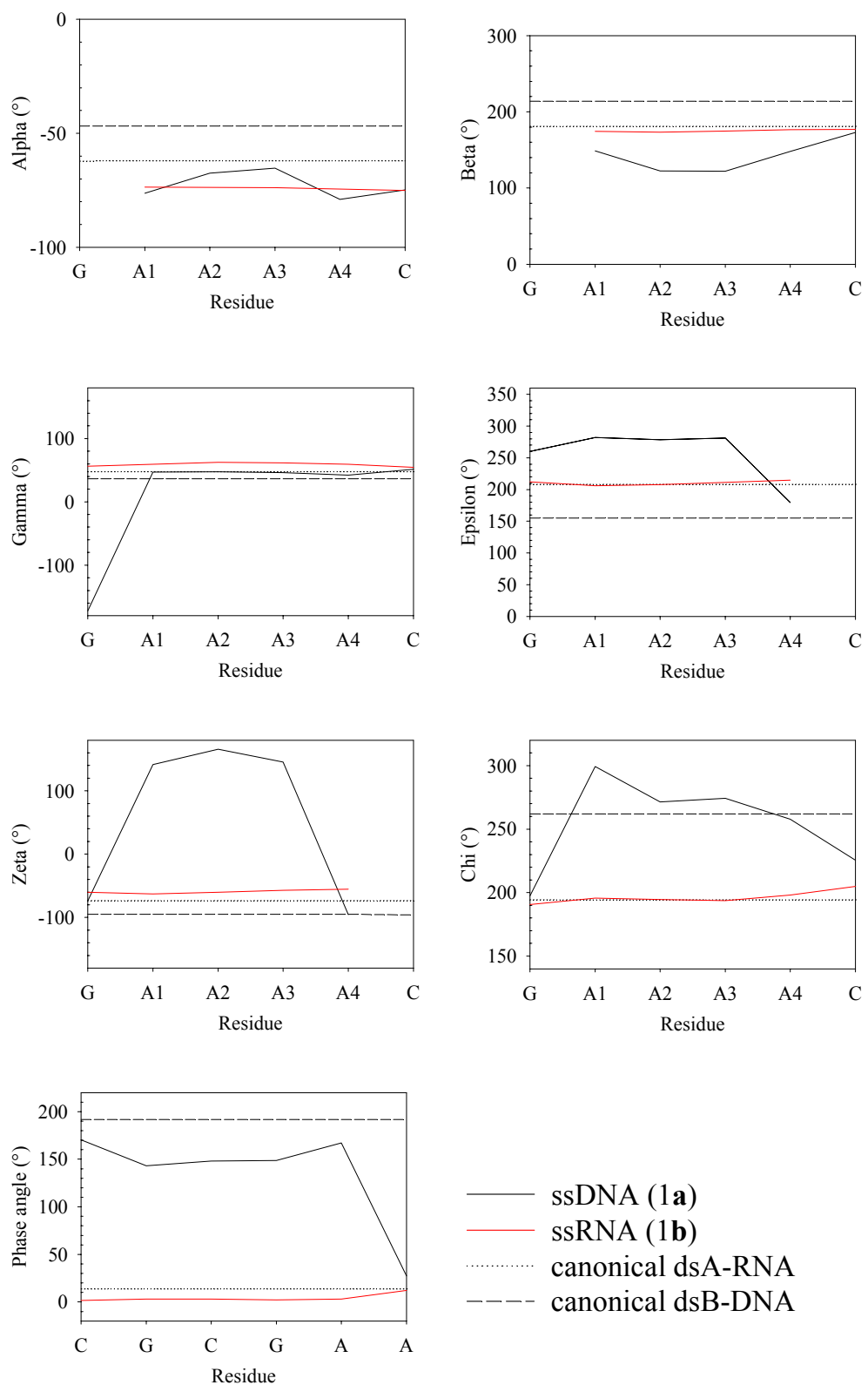
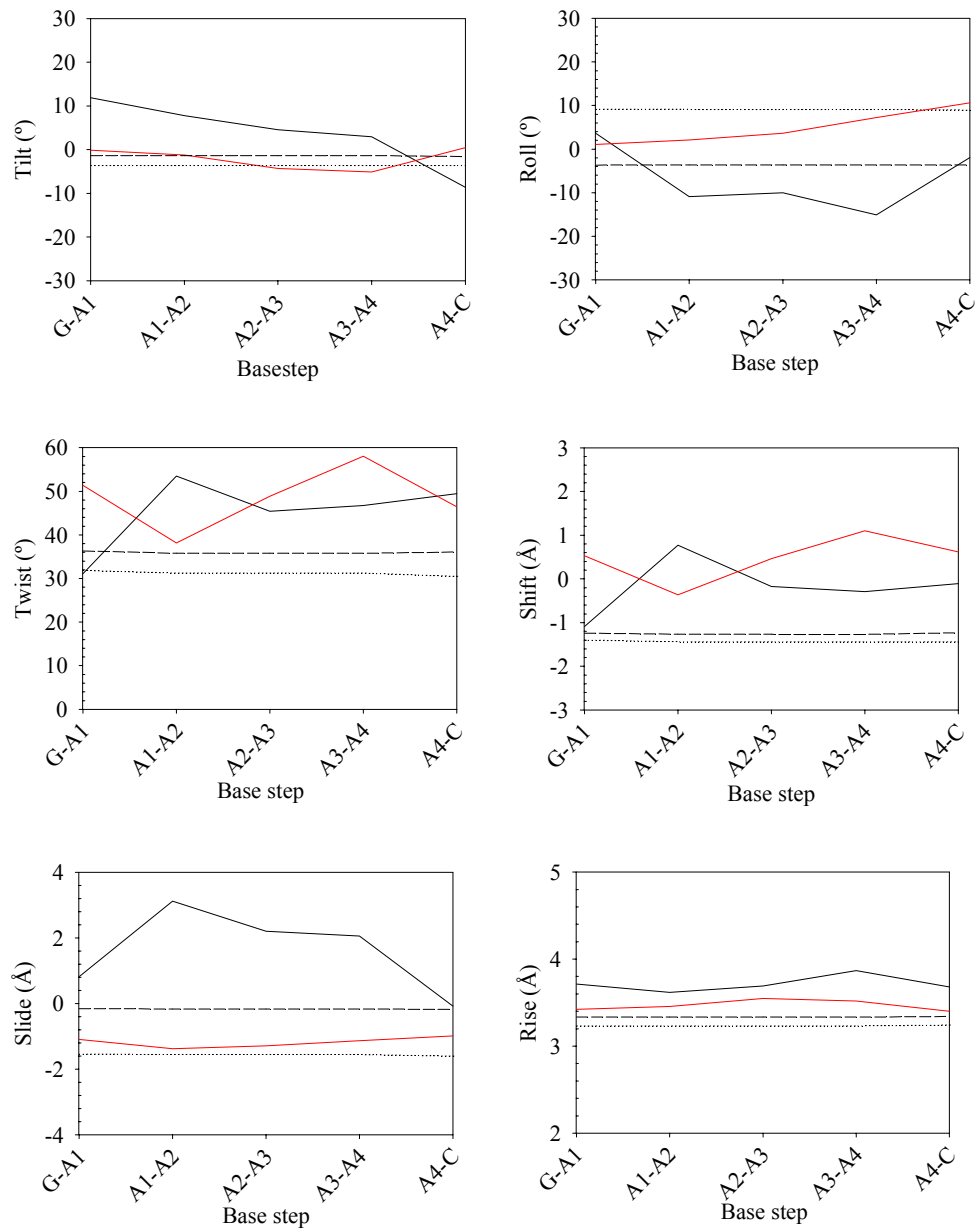


Figure S4A. A comparison of the backbone dihedrals of the average structures of the final 100 ps of the MD simulation between ssDNA (**1a**) and the ssRNA (**1b**). The average structure of the MD trajectory of the last 100 ps was based on one coordinate set per 0.15 ps, and minimized for 2000 steps using the conjugate gradient method and full NMR constraints switched on. As expected, the major differences are found for base χ torsion and the sugar phase angle (P), where ssDNA takes up the characteristic B-form and ssRNA takes up the characteristic A-form. For reference, the average values^{1a} of canonical double-stranded A-type RNA (dotted) and canonical double-stranded B-type DNA (dashed) have been plotted in the graphs.



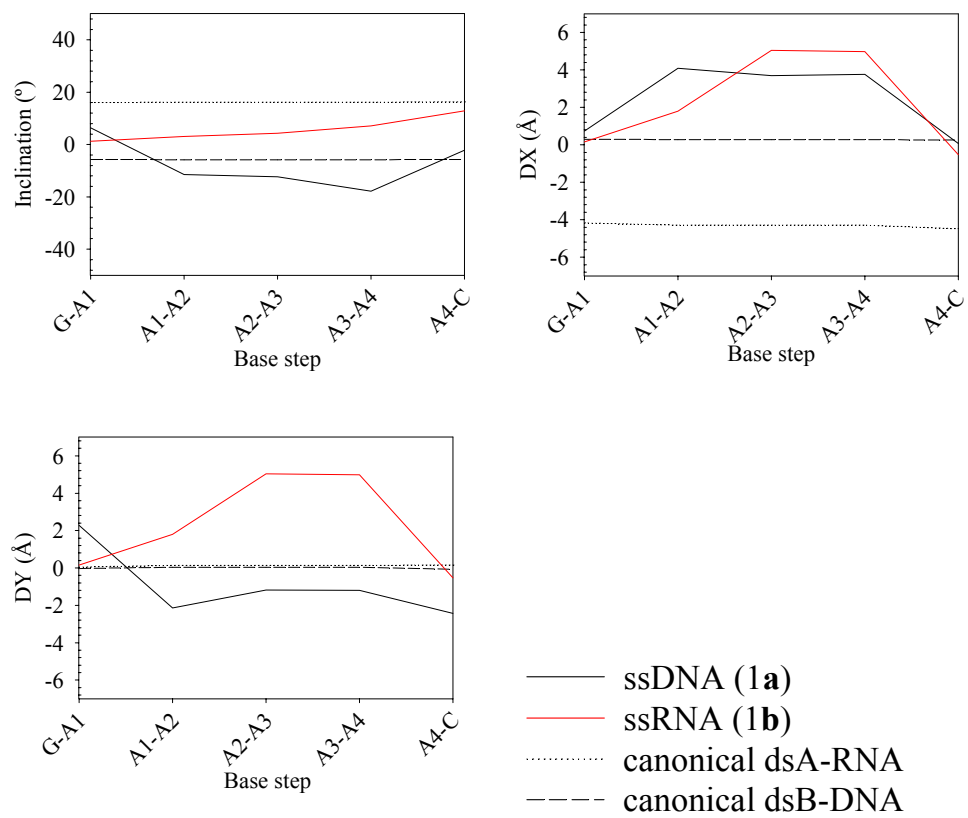


Figure S4B. A comparison between the single-strand helical parameters of the average (see experimental section) ssDNA (**1a**) and the ssRNA (**1b**) structures. Note that the software appears to define the z-axis differently for single-strands compared to duplexes (through the center), making the X-displacement comparison to the double-stranded canonical structures.

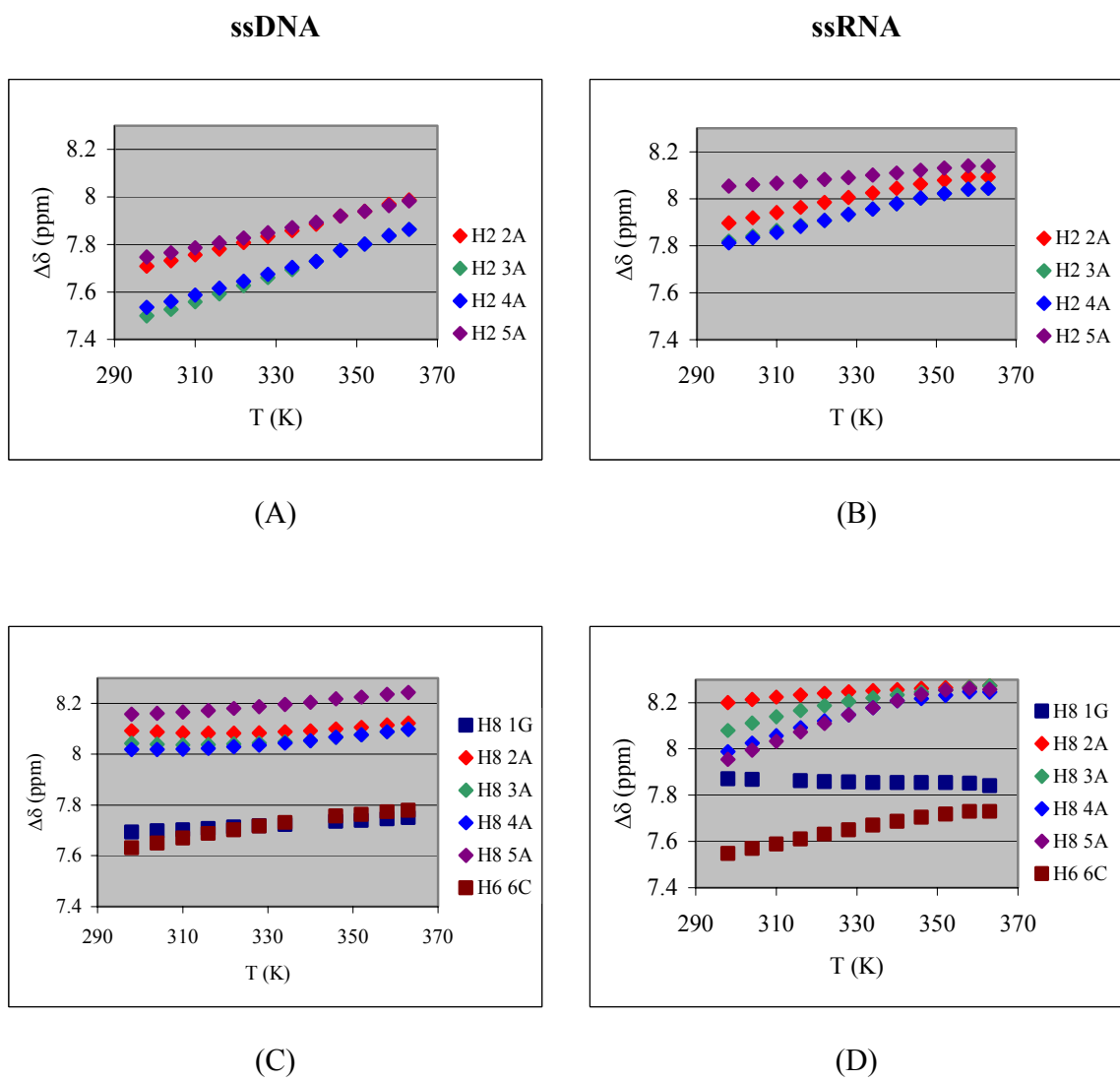


Figure S5. The left panels show the temperature-dependent drift of the ssDNA aromatic protons due to kinetically driven destacking and the right panels show the corresponding protons of ssRNA. The H2 protons in panels A and B are clearly more sensitive to destacking in ssDNA than in ssRNA, thus showing that they are more shielded in the ground state. The reverse is true for the H6/H8 protons in panels C and D that show stronger drift in ssRNA than in ssDNA. This clearly underlines the fact that the ground state stacking pattern is different in ssDNA and ssRNA.

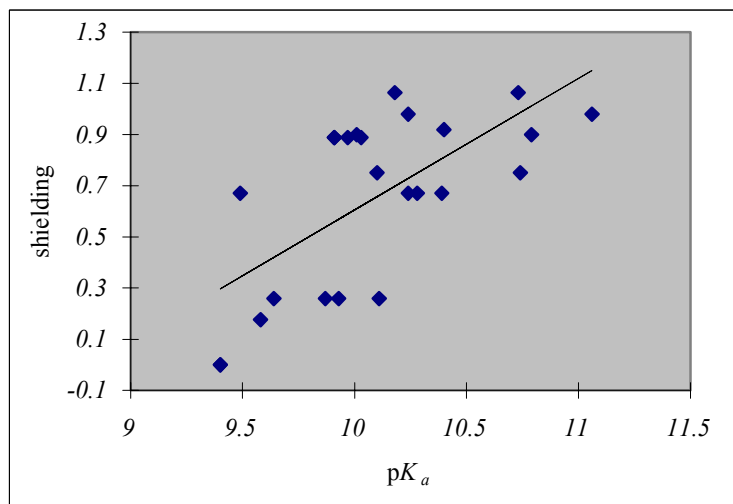


Figure S6. The shielding coefficient of the imino proton of **G** calculated using the stacking pattern for dGAAAAC and rGAAAAC plotted versus the pK_a of the following compounds: dGp, dAGA, dAGC, dCGA, dGAC, dGAAC, dGAAAAC, dCAAGAAC, dCAAGCAC, dCACGAAC, dCACGCAC, dCAAGG, rGp, rAGA, rCGA, rCGC, rGAC, rGAAAAC, rCAAGAAC, rCACGCAC, rCAAG. A correlation factor of $R = 0.66$ is found by linear regression.